Available online at www.elixirpublishers.com (Elixir International Journal)

Computational Chemistry

Elixir Comp. Chem. 89 (2015) 36678-36691

ISSN: 2229-712X

Vibrational spectroscopic (FT-IR and FT-Raman), Computational analyses of Molecular Structure and DFT Studies on O- Cresols, M- Cresols and P-Cresols

P. Dinesh

Department of Physics, Jairams Arts & Science College, Karur – 639 003, India.

ARTICLE INFO

Article history:

Received: 30 October 2015;

Received in revised form:

25 November 2015;

Accepted: 30 November 2015;

Keywords

O-Cresol,

M-cresol,

P-cresol,

FMOs,

MESP.

ABSTRACT

The structural characteristics and substituent effect of *o*-cresol, *m*-cresol and *p*-cresol have been analyzed by FTIR and FT-Raman spectroscopies. A detailed quantum chemical calculations have been performed using *ab initio* Hartree-Fock (HF) and DFT/B3LYP methods with 6-311++G(d,p) basis set. Complete vibrational analyses of the compounds were performed. The temperature dependence of thermodynamic properties has been analyzed. Molecular electrostatic potential (MESP) and frontier molecular orbitals (FMOs) are constructed at B3LYP/6-311++G(d,p) level, to understand the electronic properties. The electronic properties, HOMO and LUMO energies were also calculated. The charge density distribution and site of chemical reactivity of the molecules has been obtained by mapping electron density isosurface with electrostatic potential surfaces (ESPs).

Introduction

Cresol and its derivatives have been widely used as pharmaceuticals due to broad biological applications as antiseptics, solvents, antioxidants, etc., Now-a-days, cresol derivates have been accepted as important intermediates for the production of pesticides and insecticides, epoxy resins and dyes. In the recent years, cresol derivatives have been proved to possess attractive multifunctional properties as household cleaners and disinfectants, deodorizers [1-4]. Cresol solutions can also be found in photographic developers. *o*-cresol, *m*-cresol and *p*-cresol are used as an intermediate for organic compounds such as pharmaceuticals, pesticides and dyes [5-10].

O-cresol is used in resins, particularly epoxy cresol novolacs for microchip encapsulation, in laminates and herbicides. It is used as doddering and odor-enhancing compounds in fragrance industry [11-14]. It is also used as solvents, additives, adhesives, fiber treatment, wood preservatives, and photographic developers.

P-cresol finds use in antioxidants, polymers, elastomers, lubricants and greases. *p*-cresol belongs to the group of protein bound uremic toxins which accumulate in patients with chronic kidney disease. *p*-cresol is also used in specialty resins, UV blockers for sunscreens, fragrances and dye industries [15-17]. Typical intermediates manufactured from *p*-cresols are indoxysulfate, *p*-cresylsulfate, Indo-1, Bupranolon, 4-methylphenol and *p*-cresylglucuronate.

M-cresol is utilized in agricultural chemicals, pharmaceuticals and pressure - sensitive dyes. *m*-cresols is a precursor to the pyrethroid insecticides. *m*-cresol, either pure or mixed with *p*-cresol, is important in the production of contact herbicides such as O,O-dimethyl-O-(3-methyl-4-nitrophenyl) thino-ophosphoric acid and O,O-dimethyl-O-(3-methyl-4-methylthiophenyl) thionophoshoric acid ester. Furthermore, flavor and fragrance compounds are derived from *m*-cresols. Several important antioxidants are produced from *m*-cresol. It is also used to manufacture an explosive 2,4,6-nitro-*m*-cresol[18-21].

Considering the above mentioned aspects and the resulting demand of cresol has led to search for commercially attractive and flexible compounds and to investigate the entire properties. To the best of our knowledge, FTIR and FT-Raman vibrational studies on the fundamental modes and electronic property investigations by NBO analysis, frontier molecular orbitals (FMOs) and thermodynamic properties on *o*-cresol, *m*-cresol and *p*-cresol are inadequate in the literature. This inadequacy observed in the literature motivated us to investigate on cresols by experimental techniques and theoretical methods. Thus, a detailed investigation have been attempted using *ab initio* HF and DFT/B3LYP method with 6-311++G(d,p) basis set to provide more satisfactory and valuable information on electronic structure, molecular orbitals and potential energy distribution. The optimized geometry, FMO's and their energy gaps, molecular electrostatic potential contour (MESP), total density region and electro static potential contour (MESP) map have been constructed at B3LYP/6-311++G(d,p) level, in order to understand the electronic properties, electrophilic and nucleophilic active centers of *o*-cresol, *m*-cresol and *p*-cresol.

Experimental details

The compounds *o*-cresol, *m*-cresol and *p*-cresol were purchased from commercial sources and used without further

Tele: +91 80567 12792

E-mail addresses: pgdineshp6@gmail.com

purification to record FTIR and FT-Raman spectra. The FTIR compounds were recorded by KBr pellet method in the region 4000 - 400cm^{-1} using BROKER IFS 66V spectrometer with a Globar source, Ge/KBr beam splitter and a MCT detector. The frequencies for all sharp bands are accurate to 2cm^{-1}. The FT-Raman spectra were also recorded in the range 3500-50-cm^{-1} by the same instrument with FRA 106 Raman module equipped with Nd:YAG laser source with 200mW power operating at 1064nm. A liquid nitrogen cooled-Ge detector was used. The spectral resolution is 2 cm^{-1}.

Computational details

The first task for the computational work is to determine the optimized geometrics for the studied molecules. The stable molecular structures of *o*-cresol, *m*-cresol and *p*-cresol in the ground state is optimized and the structural parameters have been computed by *ab initio* HF and DFT-B3LYP correlation functional with 6-311++G(d,p) basis sets on a Intel core-i5 processor using GAUSSIAN 09W program [22,23]. The optimized structural parameters of *o*-cresol, *m*-cresol and *p*-cresol were used for harmonic vibrational frequency calculations resulting in IR and Raman frequencies together with intensities and Raman depolarization ratio's. The potential energy distribution of the vibrational modes of the compounds are also calculated through normal coordinate analysis [24-26] using the force constants from HF and B3LYP methods.

The Raman scattering activities (Si) calculated by Gaussian 09W program were suitably converted to relative Raman intensities (Ii) using the following relationship derived from the basic theory of Raman scattering [27].

$$I_i = \frac{f(v_0 - v_i)^4 S_i}{v_i[1 - \exp(-hcv_i / kT)]}$$

where v_o is the exciting frequency (cm^{-1}), v_i is the vibrational wavenumber of the ith normal mode, h, c and k are universal constants, and f is the suitably chosen common scaling factor for all the peak intensities. The thermodynamic parameters entropy, heat capacity at constant pressure and enthalpy change of *o*-cresol, *m*-cresol and *p*-cresol at different temperatures ranging from 100 to 1000 K were determined to study the dependence of these properties with temperature using B3LYP/6-311++G(d,p) method. Isoelectronic molecular electrostatic potential surfaces (MEPSs) and electron density surfaces [28] were calculated using 6-311++G(d,p) basis set. MESP at a point 'r' in the space around a molecule (in atomic units) can be expressed as:

$$V(r) = \sum_A \frac{Z_A}{|R_A - r|} - \int \frac{\rho(r)dr'}{|r' - r|}$$

where Z_A is the charge on nucleus A, located at R_A and $\rho(r')$ is the electronic density function for the molecule. The first and second terms represent the contributions to the potential due to nuclei and electrons, respectively. V(r) is the resultant at each point r, which is the net electrostatic effect produced at the point r by both the electrons and nuclei of the molecule. MESP serves as a useful quantity to explain hydrogen bonding, reactivity and structure–activity relationship of molecules including biomolecules and drugs [29]. Structures resulting from the plot of electron density surface mapped with electrostatic potential surface depict the shape, size, charge density distribution and the site of chemical reactivity of a molecule. Gauss View 5.0.8 visualization program [30] has been used to construct the MESP surface, the shape of highest occupied molecular orbital (HOMO) and lowest unoccupied molecular orbital (LUMO) orbitals. The energies of the HOMO and LUMO molecular orbitals [31] and HOMO–LUMO energy gap have also been measured by B3LYP/6-311++G(d,p) method [32–36].

Results and discussions

Structural properties

The optimized molecular structures of *o*-cresol, *m*-cresol and *p*-cresol along with numbering of atoms are shown in Fig 1.

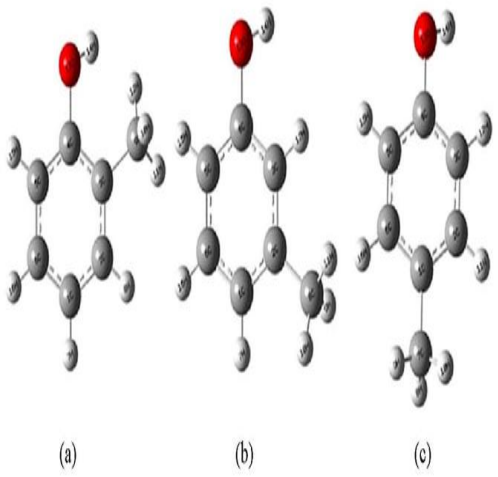

Fig 1. The structure and atom numbering scheme of (a) o-cresol, (b) m-cresol and (c) p-cresol.

The global minimum energy obtained by *ab initio* HF and DFT-B3LYP for the optimized structure of *o*-cresol; *m*-cresol and *p*-cresol are presented in Table 1.

Table 1. Total energies (in Hartrees) of *o*-cresol, *m*-cresol and *p*-cresol calculated at *ab initio* HF and DFT/B3LYP level theory.

Method/Basis set	*o*-cresol	*m*-cresol	*p*-cresol
HF/6-311++G(d,p)	-344.541699088	-344.542881277	-344.536441160
B3LYP/6-311++G(d,p)	-346.785410613	-346.785754807	-346.784930417

The optimized structural parameters bond lengths and bond angles for the thermodynamically preferred geometry of *o*-cresol, *m*-cresol and *p*-cresol at HF and B3LYP levels with 6-311++G(d,p) basis sets have been presented in Table 2.

Thermodynamic Properties

The energies and thermodynamic parameters of the title compounds have also been computed at HF and B3LYP methods with 6-311++G(d,p) basis set are presented in Table 3. Along with the frequency calculations, the zero point energies, thermal correction to internal energy enthalpy. Gibbs free energy and entropy as well as the heat capacity for the molecular systems are also computed. The higher total dipole moment of *p*-cresol (2.06 Debye) than that of *o*-cresol and *m*-cresol is due to more interactions of substituents.

The temperature dependence of the thermodynamic properties heat capacity at constant pressure (*Cp*), entropy (*S*) and enthalpy charge ($\Delta H_0 \rightarrow T$) of *o*-cresol, *m*-cresol and *p*-cresol were also were also determined by B3LYP/6-311++G(d,p) method and listed in Table 4. The anharmonicity effects have been eliminated by scaling the thermodynamic property by 0.93.

Table 2. Optimized geometrical parameters of *o*-cresol, *m*-cresol and *p*-cresol obtained by HF/6-311G++(d,p) and B3LYP/6-311G++(d,p)

Structural parameters	*o*-cresol		*m*-cresol		*p*-cresol	
	HF/ 6311G++ (d,p)	B3LYP/ 6-311G++(d,p)	HF/ 6311G++ (d,p)	B3LYP/ 6-311G++(d,p)	HF/ 6311G++ (d,p)	B3LYP/ 6-311G++(d,p)
Bond length(Å)						
C1-C2	1.386	1.394	1.386	1.399	1.380	1.394
C2-C3	1.387	1.400	1.387	1.396	1.392	1.400
C3-C4	1.382	1.401	1.382	1.395	1.387	1.401
C4-C5	1.390	1.407	1.390	1.399	1.397	1.407
C5-C6	1.383	1.393	1.382	1.395	1.382	1.393
C6-C1	1.398	1.396	1.398	1.408	1.386	1.396
C4-O13	1.378	1.083	1.378	1.400	1.072	1.083
O13-H14	1.072	1.513	1.072	1.084	1.509	1.513
C5-H15	1.072	1.084	1.072	1.082	1.073	1.084
C6-H16	1.072	1.081	1.072	1.083	1.070	1.081
C1-H7	1.509	1.401	1.509	1.512	1.380	1.401
C3-C9	1.084	1.072	-	-	-	-
C9-H10	1.083	1.093	-	-	-	-
C9-H11	1.070	1.081	-	-	-	-
C9-H12	1.072	1.083	-	-	-	-
C2-H8	1.070	1.084	-	-	-	-
C3-H12	-	-	1.081	1.091	-	-
C2-C8	-	-	1.083	0.972	-	-
C8-H9	-	-	1.093	1.093	-	-
C8-H10	-	-	1.083	1.093	-	-
C8-H11	-	-	1.070	1.081	-	-
C2-H11	-	-	-	-	1.070	1.084
C3-H12	-	-	-	-	1.378	1.084
C1-C7	-	-	-	-	1.509	1.512
C7-H8	-	-	-	-	1.083	0.972
C7-H9	-	-	-	-	1.093	1.091
C7-H10	-	-	-	-	1.081	1.093
Bond Angle(˚)						
C1-C2-C3	120.40	120.36	120.40	120.38	119.61	119.50
C2-C3-C4	120.94	120.94	120.94	120.96	121.41	121.40
C3-C4-C5	118.80	118.82	118.80	118.81	117.68	117.77
C4-C5-C6	120.69	120.61	120.70	120.63	121.58	121.53
C5-C6-C1	120.35	120.48	120.35	120.47	119.56	119.48
C6-C1-C2	118.76	118.76	118.81	118.76	120.19	120.32
H14-O13-C4	114.90	112.46	114.89	112.45	107.53	107.21
O13-C4-C3	122.45	122.58	122.45	122.65	120.00	119.53
O13-C4-C5	116.61	116.45	116.61	116.39	118.89	119.07
H15-C5-C4	119.38	119.45	119.38	119.41	119.43	119.40
H15-C5-C6	119.92	119.94	119.93	119.97	119.02	119.07
H16-C6-C5	119.90	119.87	119.90	119.88	121.51	121.52
H16-C6-C1	119.75	119.65	119.74	119.65	118.93	118.99
H7-C1-C6	111.05	111.05	111.32	111.38	114.88	112.44
H7-C1-C2	111.05	111.37	111.05	111.27	111.17	111.23
C9-C3-C2	120.44	120.45	-	-	-	-
C9-C3-C4	120.70	120.82	-	-	-	-
C3-C9-H10	111.05	111.27	-	-	-	-
C3-C9-H11	121.25	121.08	-	-	-	-
C3-C9-H12	118.89	119.07	-	-	-	-
H8-C2-C1	114.88	112.44	-	-	-	-
H8-C2-C3	118.34	118.53	-	-	-	-
C8-C2-C1	-	-	120.84	120.51	-	-
C8-C2-C3	-	-	118.81	118.76	-	-
C2-C8-H9	-	-	111.05	111.37	-	-
C2-C8-H10	-	-	107.75	107.56	-	-
C2-C8-H11	-	-	121.25	121.08	-	-
H12-C3-C2	-	-	120.65	120.06	-	-
H12-C3-C4	-	-	120.54	120.57	-	-
C7-C1-C2	-	-	-	-	120.84	120.51
C7-C1-C6	-	-	-	-	120.36	120.72
C1-C7-H8	-	-	-	-	111.05	111.05
C1-C7-H9	-	-	-	-	111.05	111.27
C1-C7-H10	-	-	-	-	111.32	111.47
H11-C2-C1	-	-	-	-	118.35	118.54
H11-C2-C3	-	-	-	-	121.25	121.08

Table 3. Thermodynamic parameters of *o*-cresol, *m*-cresol and *p* –cresol.

Parameter	*o*-cresol		*m*-cresol		*p*-cresol	
	6-311++G(d,p)		6-311++G(d,p)		6-311++G(d,p)	
	HF	B3LYP	HF	B3LYP	HF	B3LYP
Zero-point vibrational Energy (kJ/mol)	84.3125	82.66081	88.43101	82.58492	88.43940	82.71164
Rotational constants (GHz)	3.70015	3.20500	3.70015	5.48090	5.58512	3.64563
	1.80599	2.18604	1.80598	1.44054	1.46245	1.77181
	1.22267	1.31024	1.22266	1.14882	1.16721	1.20118
Thermal energy (kJ/mol)						
Total	92.801	87.277	92.801	87.235	92.821	87.323
Translational	0.889	0.889	0.889	0.889	0.889	0.889
Rotational	0.889	0.889	0.889	0.889	0.889	0.889
Vibrational	91.024	85.500	91.024	85.458	91.043	85.545
Molar capacity at constant volume ($calmol^{-1}Kelvin^{-1}$)						
Total	25.821	27.899	25.821	27.918	25.818	27.804
Translational	2.981	2.981	2.981	2.981	2.981	2.981
Rotational	2.981	2.981	2.981	2.981	2.981	2.981
Vibrational	19.859	21.938	19.860	21.956	19.856	21.842
Entropy ($calmol^{-1}Kelvin^{-1}$)						
Total	83.264	83.544	83.268	84.831	82.971	84.539
Translational	39.949	39.949	39.949	39.949	39.949	39.949
Rotational	28.066	27.951	28.066	27.963	27.913	28.118
Vibrational	15.249	15.644	15.252	16.919	15.108	16.472
Dipole moment (Debye)						
μ_x	-0.0061	-0.9740	-0.0059	-0.8477	-0.9895	-1.6132
μ_y	1.5263	-1.7790	1.5263	1.5379	.6002	-1.2858
μ_z	0.0000	0.0007	-0.0008	0.0000	0.0000	0.0006
μ_{total}	1.5263	2.0282	1.5263	1.7561	1.8815	2.0629

Table 4. Temperature dependence of the thermodynamic properties of *o*-cresol, *m*-cresol and *p*-cresol determined by DFT/B3LYP 6-311++G(d,p) method.

T (K)	*o*-cresol			*m*-cresol			*p*-cresol		
	S ($J.mol^{-1}.K^{-1}$)	Cp ($J.mol–1.K^{-1}$)	$\Delta H_0 \rightarrow T$ ($kJ.mol^{-1}$)	S ($J.mol^{-1}.K^{-1}$)	Cp ($J.mol–1.K^{-1}$)	$\Delta H_0 \rightarrow T$ ($kJ.mol^{-1}$)	S ($J.mol^{-1}.K^{-1}$)	Cp ($J.mol–1.K^{-1}$)	$\Delta H_0 \rightarrow T$ ($kJ.mol^{-1}$)
100	63.0393	8.7547	7.9498	66.7863	8.8960	7.9496	63.2568	9.8073	7.9521
200	69.1084	13.9919	8.0450	72.9617	15.3824	8.0540	69.9114	16.7320	8.1818
298.15	72.9982	19.8293	8.2939	77.0293	23.3934	8.3948	73.9985	24.9833	8.6940
300	73.8634	22.2833	8.4300	78.0421	24.7306	8.5140	75.6762	25.0361	8.9844
400	78.6806	31.2789	9.2074	83.3536	34.1361	9.4610	81.6211	33.6024	10.3610
500	83.8585	39.5140	10.4028	89.1213	42.3454	10.9092	87.9224	41.3402	12.2447
600	89.4291	46.5320	12.0045	95.3268	49.1363	12.8265	94.5748	47.9267	14.5760
700	95.3490	52.3959	13.9829	101.8964	54.7100	15.1642	101.5271	53.4561	17.3016
800	101.5578	57.3013	16.3006	108.7533	59.3271	17.8705	108.7215	58.1137	20.3715
900	107.9979	61.4327	18.9185	115.8312	63.1974	20.8962	116.1057	62.0641	23.7406
1000	114.6196	64.9361	21.7998	123.0765	66.4737	24.1973	123.6361	65.4350	27.3692

Figs. 2 - 4 depict the correlation of heat capacity at constant pressure (*Cp*), entropy (*S*) and enthalpy charge ($\Delta H_0 \rightarrow T$) with temperature along with the correlation equations and also depict the entropies, heat capacities, and enthalpy charges were increasing with temperature due to the fact that the molecular vibrational intensities increase with temperature [37].These observed relations of the thermodynamic functions vs. temperatures were fitted by quadratic formulas and the corresponding fitting repression factors (R2) are all not less than 0.996.

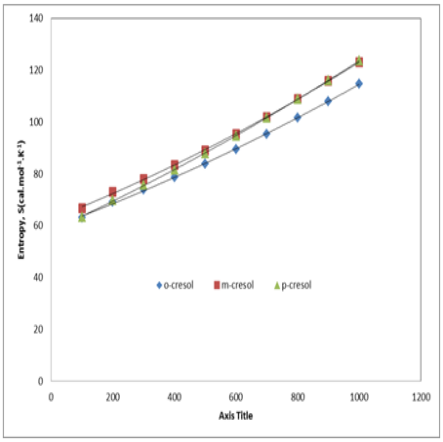

Fig 2. Temperature dependence of entropy of *o*-cresol, *m*-cresol and *p*-cresol

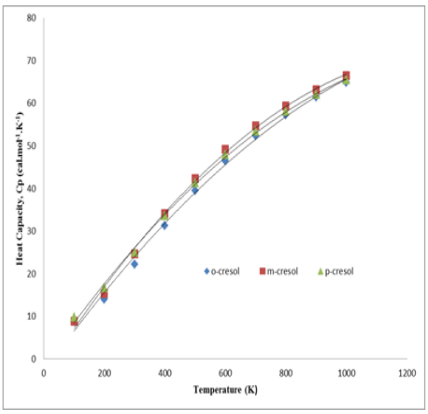

Fig 3. Temperature dependence of heat capacity of *o*-cresol, *m*-cresol and *p*-cresol

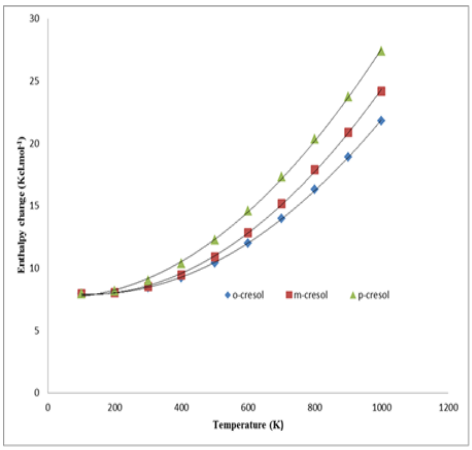

Fig 4. Temperature dependence of enthalpy of *o*-cresol, *m*-cresol and *p*-cresol

The corresponding relation between the thermodynamic parameters and temperatures for *o*-cresol are

$C^{\circ}_{p,m}$ = -3.09846 + 0.09973017 T - 3.080451226 x 10^{-5} T^2 (R^2 = 0.996302316)

S°_{m} = 1.11765E-05 + 0.044099629 T + 59.19262155 x 10^{-5} T^2 (R^2 = 0.999532823)

ΔH°_{m} = 1.8369 - 0.004687917 T + 8.21041883 x 10^{-5} T^2 (R^2=0.999856526)

for *m*-cresol the corresponding equations are

$C^{\circ}_{p,m}$ = -4.05854 + 0.110971148 T - 3.575274751 x 10^{-5} T^2 (R^2 = 0.997615462)

S°_{m} = 1.37972 + 0.046767826 T + 62.48067576 x 10^{-5} T^2 (R^2 = 0.99976024)

ΔH°_{m} = 2.10526 - 0.004858922 T + 8.15139171 x 10^{-5} T^2 (R^2 = 0.999718019)

and for *p*-cresol the corresponding equations are

$C^{\circ}_{p,m}$ = -3.49801 + 0.102084793 T - 1.327936131 (R^2=0.998604323)

S°_{m} = 1.11971 + 0.054251158 T + 58.14631161 (R^2=0.999858208)

ΔH°_{m} = 2.12673 - 0.001348314 T + 7.661928059 (R^2=0.999468724)

All these thermodynamic parameters of all these compounds are very closer to each other.

Analysis of frontier molecular orbitals (FMOs) and molecular electrostatic potentials

The molecular electrostatic potential surface (MESP) which is a method of mapping electrostatic potential onto the iso-electron density surface simultaneously displays electrostatic potential for positive and negative potentials of *o*-cresol, *m*-cresol and *p*-cresol are shown in Figs. 5–7.

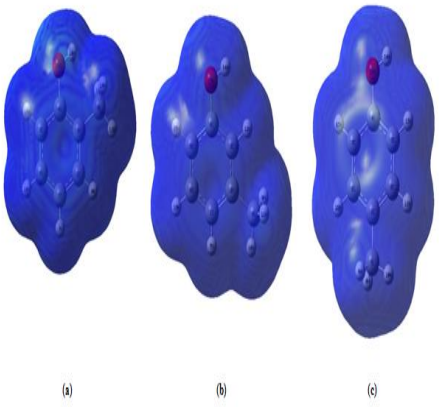

Fig 5. The isosrface mapped with total electron density of (a) *o*-cresol, (b) *m*-cresol and (c) *p*-cresol

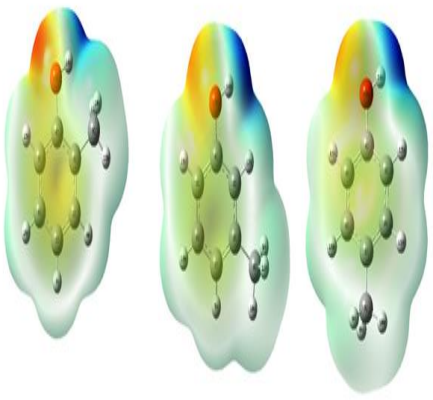

Fig 6. The total electron density mapped with electrostatic potential isosurface of (a) *o*-cresol, (b) *m*-cresol and (c) *p*-cresol

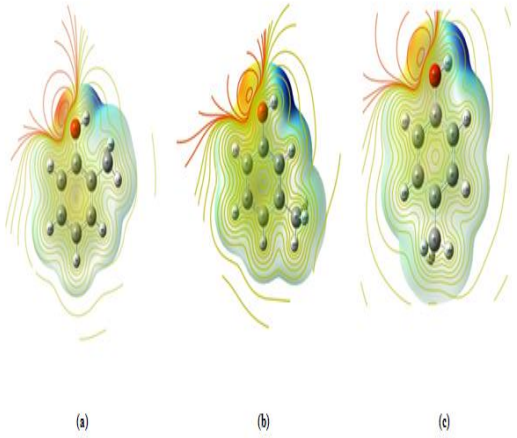

Fig 7. The electrostatic potential contour map of (a) *o*-cresol, (b) *m*-cresol and (c) *p*-cresol

The color scheme for the MESP surface is red, electron rich, partially negative charge; blue, electron deficient, partially positive charge; light blue, slightly electron deficient region; yellow, slightly electron rich region; green, neutral; respectively.

In principle, there are several ways to calculate the excitation energies. The simplest one involves the difference between the highest occupied molecular orbital (HOMO) and the lowest unoccupied molecular orbital (LUMO) of a neutral system, which is a key parameter in determining molecular properties [38]. Moreover, the eigenvalues of HOMO (π donor) and LUMO (π acceptor) and their energy gap reflect the chemical activity of the molecules. Recently, the energy gap between HOMO and LUMO has been used to prove the bioactivity from intra-molecular charge transfer (ICT) [39, 40]. The molecular orbital (MO) calculations indicate that the title compound has 88 occupied MOs. The HOMO-LUMO energy gap of *o*-cresol, *m*-cresol and *p*-cresol was calculated at *ab initio* HF and DFT-B3LYP methods using 6-311++G(d,p) basis sets and they are shown in Table 5. The frontier molecular orbitals (FMOs) of *o*-cresol, *m*-cresol and *p*-cresol, with their energies are plotted in Fig 8.

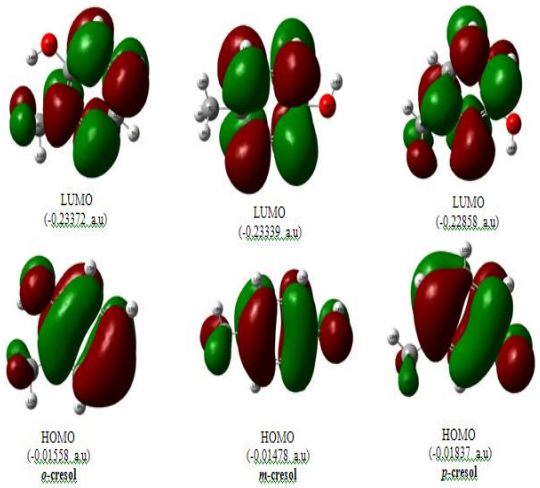

Fig 8. The frontier molecular orbitals of (a) *o*-cresol, (b) *m*-cresol and (c) *p*-cresol

The positive and negative phase is represented in red and green colour, respectively. From the plots we can see that the region of HOMO spread over the entire molecules. The calculated energy gap of HOMO–LUMO's explains the ultimate charge transfer interface within the molecule.

Table 5. Calculated HOMO-LUMO energies using HF and DFT methods

Compound	Parameters	HF 6-311++G(d, p)	B3LYP 6-311++G(d, p)
o-cresol	HOMO energy (a.u)	-0.31958	-0.23372
	LUMO energy (a.u)	-0.03732	-0.01558
	HOMO-LUMO energy gap (a.u)	-0.28226	-0.21814
m-cresol	HOMO energy (a.u)	-0.31958	-0.23339
	LUMO energy (a.u)	-0.03732	-0.01478
	HOMO-LUMO energy gap (a.u)	-0.28226	-0.21021
p-cresol	HOMO energy (a.u)	-0.31295	-0.22858
	LUMO energy (a.u)	-0.03686	-0.01837
	HOMO-LUMO energy gap (a.u)	-0.21021	-0.21021

Natural bond orbital analysis

Natural bond orbital (NBO) analysis originated as a technique for studying hybridization and covalency effects in polyatomic wave functions, based on local block Eigen vectors of the one-particle density matrix. NBOs would correspond closely to the picture of localized bonds and lone pairs as basic units of molecular structure. The atomic charges of *o*-cresol, *m*-cresol and *p*-cresol calculated by NBO analysis using B3LYP/6-311++G(d,p) methods are presented in the Table 6.

The correlation of atomic charges of *o*-cresol, *m*-cresol and *p*-cresol are depicted in the Fig. 9.

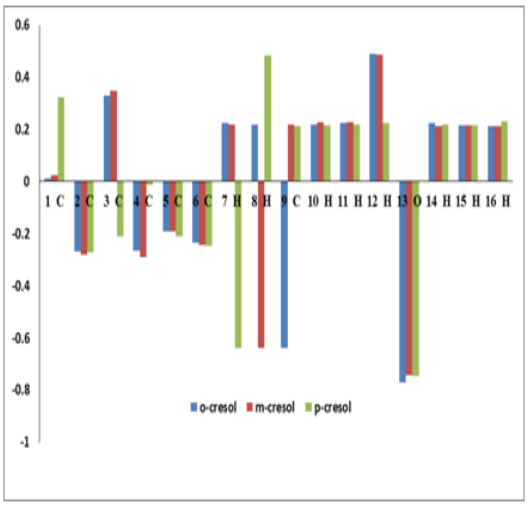

Fig 9. The correlation of atomic charges of *o*-cresol, *m*-cresol and *p*-cresol

Vibrational Spectra

From the spectral point of view, the title compound is assumed to have C_s point group symmetry. The 42 fundamental modes of vibrations arising for the title compounds are classified into 28 A' and 14 A" species. The A' and A" species represent in-plane and out-of-plane vibrations, respectively.

It is well known that the harmonic frequencies by *ab initio* HF and DFT calculations are usually higher than the corresponding experimental quantities due to the fact of the electron correlation approximate treatment, anharmonicity effects and basis set deficiencies etc, [41]. A better agreement between the computed and experimental frequencies can be obtained by using different scale factors for different regions of vibrations.

Table 6. The natural charges of the atoms of *o*-cresol, *m*-cresol and *p*-cresol determined by natural bond analysis (NBO) using B3LYP/6-311++G(d,p) method

Atom	*o*-cresol	Atom	*m*-cresol	Atom	*p*-cresol
1 C	0.01251	1 C	0.02380	1 C	0.32424
2 C	-0.26908	2 C	-0.27995	2 C	-0.27350
3 C	0.32933	3 C	0.34660	3 C	-0.21161
4 C	-0.26477	4 C	-0.28989	4 C	-0.01358
5 C	-0.19276	5 C	-0.19048	5 C	-0.21098
6 C	-0.23530	6 C	-0.24421	6 C	-0.24616
7 H	0.22515	7 H	0.21909	7 C	-0.63754
8 H	0.21946	8 C	-0.63777	8 H	0.48468
9 C	-0.63830	9 H	0.21874	9 H	0.21250
10 H	0.21963	10 H	0.22667	10 H	0.21445
11 H	0.22279	11 H	0.22796	11 H	0.21680
12 H	0.48833	12 H	0.48485	12 H	0.22418
13 O	-0.77114	13 O	-0.74515	13 O	-0.74543
14 H	0.22467	14 H	0.21145	14 H	0.21746
15 H	0.21622	15 H	0.21611	15 H	0.21548
16 H	0.21326	16 H	0.21216	16 H	0.22902

The correction factors used to correlate the experimentally observed and theoretically computed frequencies for each vibration by HF and DFT/B3LYP methods are similar and an explanation of this approach was discussed previously [42-50]. The scale factors in this study minimized the deviations very much between the experimental and calculated frequencies at HF and B3LYP methods of calculations. The experimentally recorded FT-IR and FT-Raman spectra with theoretical simulated IR and Raman spectra for *o*-cresol, *m*-cresol and *p*-cresol are shown in Figs 10 and 11, respectively.

The observed and calculated frequencies using *ab initio* HF/6-311++G(d, p) and B3LYP using 6-311++G(d, p) force fields along with their relative intensities, probable assignments and potential energy distribution (PED) of the compounds were summarized in Tables 7-9, respectively.

O-H Vibrations

The OH group gives rise to three modes of vibration such as, stretching, in-plane bending and out-of-plane bending vibrations. The OH stretching vibrations are sensitive to hydrogen bonding [51]. The vibrational bands due to the O-H stretching are medium to strong intensity in the infrared spectrum, although it may be broad. At the same time in Raman spectrum the band is generally weak [52-53].

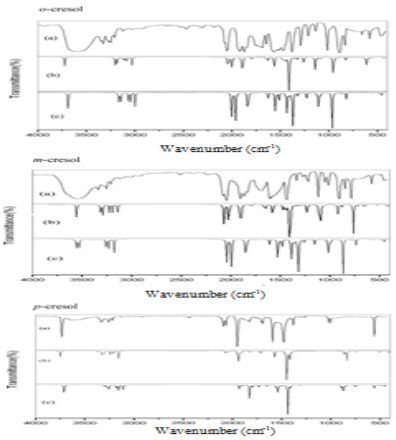

Fig 10. Comparison of observed and calculated IR spectra of *o*-cresol, *m*-cresol and *p*-cresol.
(a) observed, (b) calculated with B3LYP/6-311++G(d,p)
(c) calculated with HF/6-311++G(d,p)

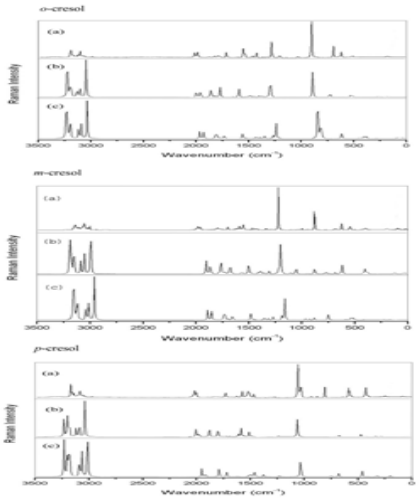

Fig 11. Comparison of observed and calculated Raman spectra of *o*-cresol, *m*-cresol and *p*-cresol.
(a) observed, (b) calculated with B3LYP/6-311++G(d,p)
(c) calculated with HF/6-311++G(d,p)

Unassociated hydroxyl groups absorb strongly in the region 3700-3584 cm^{-1} whereas the existence of intermolecular hydrogen bond formation can lower the O-H stretching frequency in the range 3500-3200 cm^{-1}, with increase in intensity and breadth. For OH groups, the strong band observed at 3408 cm^{-1} in FTIR of *o*-cresol, and weak bands observed at 3371 cm^{-1} in FT-Raman of *m*-cresol, and strong band observed at 3473 cm^{-1} in *p*-cresol are assigned to the O-H stretching modes. The in-plane O-H deformation vibration usually appears as strong band in the region 1400-1260 cm^{-1}. The theoretically predicted band at 1346 cm^{-1} of *o*-cresol, 1327 cm^{-1} of *m*-cresol and 1347 cm^{-1} of *p*-cresol are assigned to in-plane bending vibrations of O-H group. These frequency values show very good agreement with the experimental values and the frequencies calculated by other methods are also consistent with experimental values. The O-H out-of-plane deformation vibration lies in the region 280-312 cm^{-1} for free O-H and in the region 600-720 cm^{-1} for associated O-H [54]. The bands at 585, 540 and 539 cm^{-1} in the IR spectra respectively of *o*-cresol, *m*-cresol and *p*-cresol were assigned to the O-H out-of-plane bending.

C-H Vibration

The aromatic C-H stretching vibrations are normally found between 3100 and 3000 cm^{-1} frequency ranges, with multiple weak bands. The nature of substituent cannot affect much to the bands in this region [54, 55]. The Raman active bands observed at 3061, 3033 and 2960 cm^{-1} and IR active bands at 3108 and 3063 cm^{-1} have been assigned to C-H stretching mode in *o*-cresol. In *m*-cresol, the IR and Raman bands observed at 3162, 3127, 3092 and 3041 cm^{-1} are assigned to C-H stretching. Similarly, in *p*-cresol, the bands at 3069, 3053, 3041 and 3013 cm^{-1} are assigned to C-H stretching. These values are found to be in line with the calculated as well as the literature values.

The CH in-plane bending vibrations appear as sharp but weak to medium intensity band in the region 1300-1000 cm^{-1}. These bands are not sensitive to the nature of substituent [55]. The FT-Raman bands at 1267, 1157cm^{-1} and infrared bands at 1241, 1109 cm^{-1} in *o*-cresol, and the FTIR bands at 1035, 1009, 1000, 879 cm^{-1} in *m*-cresol, and FT-Raman band at 1217 cm^{-1} and FTIR 1293, 1266, 1171 cm^{-1} in *p*-cresol were assigned to C-H in-plane bending vibrations of the title compounds. The out-of-plane bending modes of vibrations have also been assigned for *o*-cresol, *m*-cresol and *p*- cresol and they are presented in Tables 7-9.

Methyl group vibration

The title molecules *o*-cresol, *m*-cresol and *p*-cresol possess a CH_3 in the third, second and first position, respectively. For the assignments of CH_3 group frequencies, basically nine fundamentals can be associated with each CH_3 group namely, CH_{3ass}; asymmetric stretch; CH_{3ss}; symmetric stretch (ie., in-plane hydrogen stretching mode); CH_{3ipb}; in-plane-bending (ie., hydrogen deformation mode); CH_{3sb}; symmetric bending ; CH_{3ipr}; in-plane-rocking; CH_{3opr}; out-of-plane rocking and tCH_3; twisting hydrogen bending modes. In addition to that, CH_{3ops}; out-of-plane stretch and CH_{3opb}; out-of-plane bending modes of the CH_3 group would be expected to be depolarized for A" symmetry species. The CH_3 stretching is observed at lower wavenumbers than the corresponding C-H stretching of an aromatic ring (3000-3100 cm^{-1}). The asymmetric C-H stretching modes of CH_3 group are expected around 2980 cm^{-1} and symmetric one is expected in the region 2870 cm^{-1} [53, 56-58]. For, o-cresol, the vibrational frequencies of 2939 and 2930 cm^{-1} (mode 6) calculated by HF/6-311++G (d, p) and B3LYP/6-311++G (d, p), respectively are assigned to CH_3 asymmetric stretching vibration in methyl group present in the molecule. The bands in the IR and Raman spectra at 2920 cm^{-1}, respectively are also assigned to those vibrations modes.

The IR band at 2861 cm^{-1} is assigned to the CH_3 symmetric stretching band. The corresponding symmetric stretching mode is computed at 2876 cm^{-1} by the HF/6-31++G (d, p) method and 2869 cm^{-1} by the B3LYP/6-311++G (d, p).

The two in-plane methyl hydrogen deformation modes are also well established. In the present investigation, we have observed the symmetrical methyl deformation mode CH_{3sb}, at 1381 and 1383 cm^{-1} in the infrared and Raman and in-plane-bending methyl deformation mode CH_{3ipb}, at 1494 cm^{-1} in IR. The theoretically computed values show an excellent agreement with experimental results. The bands at 2736 cm^{-1} and 1174 cm^{-1} in infrared are attributed to CH_{3ops} and CH_{3opb}, respectively. They show good agreement with the calculated spectral values by the HF/6-311++G(d,p) and DFT/B3LYP/6-311++G(d,p) methods. The bands obtained at 986 cm^{-1}(A') and 931 cm^{-1}(A") in IR are assigned to CH_3 in-plane and out-of-plane rocking modes. The assignment of the band at 281 cm^{-1} in Raman is attributed to methyl twisting mode and they are listed in Table 7.

Similarly, for *m*- and *p*-cresols, the same trend is observed. The calculated and observed wave numbers of CH_3 group for both molecules are listed in Tables 8 and 9.

Polarizability and hyperpolarizability

The values of the polarizability tensor components for a given system will depend on the choice of the Cartesian co-ordinate system used. The molecule for which $\alpha_{xx} = \alpha_{yy} = \alpha_{zz}$ is said to be isotropic. The polarizability is isotropic or is the same in all directions for a molecule whose electron density is spherically symmetrical. If the molecules are perfectly isotropic (p) and (E) will have the same direction and is then a simple scalar quantity. If the molecule is anisotropic $\alpha_{xx} \neq \alpha_{yy} \neq \alpha_{zz}$, (p) will no longer have the same direction as (E). The intensity of Raman scattering may be proportional to the derived polarizability components. To express the scattering intensity in terms of the derived polarizability tensor, the quantities ($\bar{\alpha}$) and the anisotropy invariant (γ) are necessary. They are constant regardless of the orientation of the molecules. The quantity ($\bar{\alpha}$) is the mean value of the three principle components of ($\bar{\alpha}$) and (γ) measures the anisotropy of the tensor. The polarizability, the first hyperpolarizability and the anisotropy polarizability invariant are computed with the numerical derivative of the dipole moment using B3LYP/6-311++G(d,p) are presented in Table 10. The definitions [59] for the isotropic polarizability is

$$(\bar{\alpha}) = \frac{1}{3}(\alpha_{xx} + \alpha_{yy} + \alpha_{zz})$$

The polarizability anisotropy invariant is

$$\gamma^2 = \frac{1}{2}[(\alpha_{xx} - \alpha_{yy})^2 + (\alpha_{yy} - \alpha_{zz})^2 + (\alpha_{zz} - \alpha_{xx})^2 + 6(\alpha^2_{xy} + \alpha^2$$

and the average hyperpolarizability is

$$\beta_{total} = \sqrt{(\beta^2{}_x + \beta^2{}_y + \beta^2{}_z)}$$

Where, α_{xx}, α_{yy} and α_{zz} are tensor components of polarizability. β_x, $\beta_y$and β_z are tensor components of hyperpolarizability.

Global and local reactivity descriptors

Based on density functional descriptors global chemical reactivity descriptors of compounds such as hardness, chemical potential, softness, electronegativity and electrophilicity index as well as local reactivity have been defined [60–64]. Pauling introduced the concept of electronegativity as the power of an atom in a compound to attract electrons to it. Hardness (η), chemical potential (μ) electronegativity (χ) and softness are defined follows.

$$\eta = \frac{1}{2}\left(\frac{\partial^2 E}{\partial N^2}\right)_{v(r)} = \frac{1}{2}\left(\frac{\partial U}{\partial N}\right)_{v(r)}$$

$$\mu = \left(\frac{\partial E}{\partial N}\right)_{v(r)}$$

Table 7. The observed FTIR, FT-Raman and calculated (Unscaled and Scaled) frequencies using HF/6-311++G (d, p) and B3LYP/6-311++G (d, p) along with their probable assignments and potential energy distribution of *o*-cresol

S.No	Symm. species	Observed Frequency (cm^{-1})		Calculated frequencies (cm^{-1})								Assignments along with PED (%)
				HF/6-311++G(d,p)				B3LYP/ 6-311++G(d,p)				
		FT-IR	FT-Raman	Unscaled	Scaled	IR Intensity	Raman Activity	Unscaled	Scaled	IR Intensity	Raman Activity	
1	A′	3408	-	3483	3426	0.02	0.39	3695	3415	0.21	1.16	OH(100)
2	A′	3108	-	3358	3127	22.85	2.47	3187	3116	11.38	1.99	CH(100)
3	A′	3063	3061	3346	3059	15.62	0.46	3182	3050	0.27	1.05	CH(100)
4	A′	3033	-	3324	3053	145.15	2.74	3161	3042	76.54	1.38	CH(98)
5	A′	2960	-	3313	2986	6.56	0.11	3150	2958	71.24	1.50	CH(98)
6	A′	2920	2923	3238	2939	7.83	0.52	3095	2930	6.73	0.40	CH_3ass(98)
7	A′	2861	-	3212	2876	4.31	0.11	3067	2869	3.54	0.09	CH_3ss(98)
8	A″	2736	-	3159	2750	0.89	6.22	3009	2728	1.01	4.75	CH_3ops(97)
9	A′	1778	-	1798	1794	2.75	10.58	2069	1785	2.96	9.65	CO(96)
10	A′	1694	-	1763	1710	0.08	2.08	1856	1702	0.14	1.37	CC(87)
11	A′	-	1639	1654	1659	17.59	0.03	1656	1646	11.51	0.33	CC(84)
12	A′	-	1616	1645	1631	3.95	20.34	1621	1620	4.76	17.97	CC(81), bCH(14)
13	A′	1611		1643	1622	99.06	0.45	1536	1606	78.53	0.16	CC(84), bCH(13)
14	A′		1595	1614	1610	11.18	0.01	1530	1602	0.73	0.09	CC(80),Rsymd(17)
15	A′	1503	-	1572	1524	7.76	0.02	1528	1502	11.14	0.08	CC(82), CH(19)
16	A′	1494	-	1467	1507	42.87	0.21	1498	1499	51.89	0.22	CH_3ipb(82)
17	A′	1465	-	1402	1489	1.39	33.01	1454	1472	0.10	0.10	CC(79), Rtrigd(19)
18	A′	1381	1383	1387	1396	17.27	5.93	1437	1388	0.92	39.45	CH_3sb(80)
19	A′	-	1367	1363	1382	0.03	0.02	1392	1374	20.61	0.55	Rsymd(73), Rasym(21)
20	A′	1342	-	1351	1355	5.09	0.38	1360	1349	9.18	2.02	Rtrigd(74), CH(18)
21	A′	1329	-	1349	1346	4.12	4.15	1359	1335	4.49	2.70	bOH(70), bCO(21)
22	A′	1300	-	1362	1318	104.82	2.43	1347	1307	138.66	1.74	Rasymd(72), bCC(19)
23	A′		1267	1244	1282	11.47	3.96	1293	1273	26.24	4.95	bCH(69), CH(21)
24	A′	1241	-	1198	1256	62.34	0.45	1215	1248	15.58	1.55	bCH(67), CC(23)
25	A′	1208	-	1196	1221	22.42	0.68	1196	1213	40.88	16.45	bCC(70), CH(19)
26	A′	1174	-	1120	1188	65.56	12.03	1164	1171	15.39	0.88	CH_3opb(69)
27	A′	-	1157	1118	1176	15.28	0.33	1092	1164	6.36	0.51	bCH(70), CC(13)
28	A′	1109	-	1091	1121	2.22	8.22	1038	1115	6.60	18.05	bCH(69), CH(20)
29	A′	1044	1048	1011	1065	0.69	2.14	1025	1054	0.07	2.49	ωCC(64), OH(17)
30	A′	986	-	1008	1003	9.79	14.02	979	981	23.95	0.21	CH_3ipr(68)
31	A′	931	-	992	944	12.60	0.55	939	925	10.32	12.98	CH_3opr(69)
32	A″	844	-	882	861	47.65	7.34	899	852	37.66	6.88	ωCH(59), ωCC(21)
33	A″	-	825	864	842	78.19	14.04	887	831	58.41	13.24	ωCH(53), tRasym(19)
34	A″	-	760	798	777	75.25	18.02	785	756	52.78	16.74	ωCH(57), CH(23)
35	A″	752	-	756	763	38.18	186.29	746	759	32.68	231.04	ωCH(53), tRsym(21)
36	A″	712	-	739	723	28.20	78.02	738	708	25.27	81.06	tRtrig(59), ωCH(17)
37	A″	-	688	635	699	27.70	56.31	678	684	20.62	59.50	bCO(62), OH(23)
38	A″	-	631	589	643	1.43	67.69	571	633	4.92	77.10	tRsym(53), tRtrig(23)
39	A″	585	-	569	597	33.57	52.02	550	588	27.70	57.40	ωOH(51), Rasym(23)
40	A″	526	-	508	538	28.96	141.29	532	520	30.08	109.28	tRasym(55), ωCO(21)
41	A″	442	-	476	454	4.49	112.67	459	437	1.06	168.39	ωCO(54), ωOH(23)
42	A″	-	281	256	292	69.94	104.61	296	283	37.01	142.21	τCH_3(61)

Table 8. The observed FTIR, FT-Raman and calculated (Unscaled and Scaled) frequencies using HF/6-311++G (d, p) and B3LYP/6-311++G (d, p) along with their probable assignments and potential energy distribution of *m*-cresol

S.No	Symm. species	Observed Frequency (cm^{-1})		Calculated frequencies (cm^{-1})								
				HF/6-311++G(d,p)				B3LYP/ 6-311++G(d,p)				Assignments along
		FT-IR	FT-Raman	Unscaled	Scaled	IR Intensity	Raman Intensity	Unscaled	Scaled	IR Intensity	Raman Intensity	with PED (%)
1	A′	-	3371	3358	3395	0.02	0.39	3695	3380	0.00	0.03	OH(100)
2	A′	-	3162	3346	3181	22.86	2.47	3189	3160	0.07	12.24	CH(100)
3	A′	3127	-	3324	3114	15.67	0.46	3181	3133	0.13	0.81	CH(100)
4	A′	3092	-	3313	3110	145.08	2.74	3159	3096	0.17	6.22	CH(99)
5	A′	3041	-	3238	3028	6.56	0.11	3150	3043	0.06	139.18	CH(98)
6	A′	2954	-	3212	2973	7.83	0.52	3096	2963	0.36	6.35	CH_3ass(98)
7	A′	2950	-	3159	2968	4.31	0.11	3064	2956	0.36	3.70	CH_3ss(98)
8	A″	2860	-	2904	2877	0.89	6.22	3011	2866	0.96	1.21	CH_3ops(98)
9	A′	1824	1830	1798	840	2.75	10.59	1904	1832	1.08	2.69	CO(97)
10	A′	1690	1687	1764	1707	0.08	2.08	1656	1698	0.72	0.05	CC(87)
11	A′	-	1592	1654	1613	17.59	0.03	1621	1599	0.82	10.45	CC(86)
12	A′	-	1557	1645	1573	3.95	20.34	1538	1566	2.07	4.54	CC(83), Rtrigd(19)
13	A′	1539	-	1643	1552	99.05	0.45	1529	1547	0.49	80.88	CC(84), bCH(13)
14	A′	1517	-	1614	1529	11.18	0.01	1528	1524	0.61	0.53	CC(80), CH(16)
15	A′	1492	-	1572	1512	7.77	0.02	1498	1498	0.62	11.28	CH3ipb(85)
16	A′	1463	-	1467	1483	42.87	0.21	1452	1469	1.76	50.90	CC(79), Rsymd(20)
17	A′	-	1454	1402	1476	1.39	32.97	1359	1463	0.72	0.11	CC(83), CH3sb(84)
18	A′	1440	-	1367	1457	17.27	5.95	1347	1448	2.56	1.41	,Rtrigd(79)
19	A′	1337	1333	1297	1353	0.03	0.02	1338	1343	1.10	27.14	Rasymd(20)
20	A′	1313	-	1275	1327	5.09	0.38	1293	1322	1.06	5.33	bOH(71), bCO(19)
21	A′	1279	-	1243	1298	4.11	4.16	1215	1288	1.20	3.19	Rasym(70),bCC(23)
22	A′	1267	-	1198	1288	104.96	2.42	1196	1275	1.23	144.87	Rsymd(69),CC(19)
23	A′	1249	-	1196	1266	11.46	3.97	1165	1257	1.28	22.57	bCC(68)
24	A′	1166	-	1120	1185	62.27	0.45	1120	1174	1.03	14.49	CH3opb(70)
25	A′	1085	-	1118	1097	22.28	0.68	1093	1042	3.46	35.56	bCH(70), Rsymd(19)
26	A′	1009	-	1091	1022	65.64	12.04	1038	1016	4.13	17.76	bCH(67)
27	A′	1000	-	1011	1014	15.26	0.33	1023	1009	1.65	4.86	bCH(64),C(21)
28	A′	-	975	1008	989	2.22	8.22	976	983	1.52	7.00	CH3ipr(70)
29	A′	927	-	992	943	0.70	2.14	940	932	2.55	0.18	CH3opr(69)
30	A′	879	-	882	891	9.79	14.02	899	888	3.12	22.45	bCH(66)
31	A′	864	-	868	877	12.58	0.55	886	873	1.44	10.55	ωCC(65)
32	A″	776	760	798	788	47.59	7.35	785	782	1.73	38.63	ωCH(59)
33	A″	732	-	756	747	78.26	14.03	746	739	8.08	60.38	ωCH(57),tRasym(21)
34	A″	-	696	741	710	75.19	18.02	696	693	9.19	52.98	ωCH(54),CC(19)
35	A″	689	-	704	702	38.18	186.29	674	683	5.54	34.50	bCO(53)
36	A″	643	-	635	657	28.20	78.02	659	640	6.08	22.19	ωCH(52),tRsym(19)
37	A′	-	605	589	620	27.70	56.32	569	603	6.20	22.25	tRtrig(57), tRsym(25)
38	A″	540	-	569	551	1.44	67.70	550	543	6.36	3.34	ωOH(56)
39	A″	-	454	508	467	33.56	52.02	532	456	6.42	29.11	tRasym(52), CH(21)
40	A″	449	-	476	464	28.97	141.22	459	444	6.54	28.65	ωCO(57)
41	A″	433	-	318	448	4.48	112.72	442	429	6.54	2.59	tRsym(54)
42	A″	-	299	285	309	69.93	104.62	300	302	8.58	36.85	τCH3(60)

Table 9. The observed FTIR, FT-Raman and calculated (Unscaled and Scaled) frequencies using HF/6-311++G (d, p) and B3LYP/6-311++G (d, p) along with their probable assignments and potential energy distribution of *p*-cresol.

S.No	Symm. Species	Observed Frequency (cm^{-1})		Calculated frequencies (cm^{-1})								Assignments along with PED (%)
				HF/6-311++G(d,p)				B3LYP/ 6-311++G(d,p)				
		FT-IR	FT-Raman	Unscaled	Scaled	IR Intensity	Raman Activity	Unscaled	Scaled	IR Intensity	Raman Activity	
1	A′	3473	-	3699	3495	0.17	0.73	3695	3479	0.14	0.53	OH(100)
2	A′	-	3069	3655	3088	1.14	0.16	3198	3073	2.29	0.11	CH(100)
3	A′	3053	-	3327	3060	144.49	1.88	3168	3049	176.90	2.05	CH(100)
4	A′		3041	3189	3052	3.15	0.04	3156	3046	3.43	0.03	CH(98)
5	A′	3013	3013	3157	3020	8.12	2.96	3146	3011	7.44	3.35	CH(98)
6	A′	2946	-	3003	2967	11.19	0.83	3088	2955	12.32	0.71	CH3ass(98)
7	A′	2925	-	2290	2942	1.21	0.02	3059	2932	1.34	0.01	CH3ss(98)
8	A″	2866	-	2173	2882	3.48	9.53	3007	2859	3.72	10.42	CH3ops(98)
9	A′	1869	-	1725	1887	21.64	0.02	2350	1875	25.12	0.00	CO(98)
10	A′	1634	-	1643	1652	0.34	5.96	1965	1641	0.40	6.34	CC(92)
11	A′	1618	-	1634	1640	0.22	1.65	1653	1624	0.20	1.77	CC(90)
12	A′	-	1613	1629	1628	17.13	0.46	1629	1616	12.03	1.49	CC(87)
13	A′	-	1600	1598	1619	58.57	0.01	1579	1595	12.66	44.14	CC(1), Rtrigd(17)
14	A′	1598	-	1573	1612	12.82	39.28	1555	1574	78.27	0.12	CC(80), CH(13)
15	A′	1560	-	1570	1580	17.13	0.02	1534	1556	18.74	0.09	CC(79),bCH(15)
16	A′	1555	-	1538	1569	0.01	0.20	1530	1558	1.02	0.24	CC(80)
17	A′	1515	-	1514	1538	0.08	0.13	1462	1521	3.33	2.23	CH3ipb(84)
18	A′	1443	-	1457	1459	0.24	2.39	1452	1449	0.04	0.03	Rsymd(74), trigd(21)
19	A′	1426	-	1426	1440	0.47	0.12	1377	1434	0.15	0.14	Rtrigd(73),bCH(12)
20	A′	1381	1383	1385	1393	5.49	0.06	1215	1388	4.30	0.22	CH3sb(80)
21	A′	1338		1362	1354	70.29	2.89	1167	1343	17.85	0.32	Rasym(72), bCO(13)
22	A′	1328	-	1351	1347	179.37	11.15	1344	1332	185.63	4.71	bOH(69), CO(13)
23	A′	1293	-	1339	1307	4.33	3.05	1265	1299	10.91	1.85	bCH(69), CH(21)
24	A′	1266	-	1262	1280	1.24	18.79	1240	1272	1.23	15.38	bCH(67), CC(23)
25	A′	-	1259	1261	1271	38.06	6.31	1141	1263	81.90	7.92	bCC(70), CH(21)
26	A′	-	1217	1191	1226	2.90	1.28	1092	1214	24.15	3.88	bCH(69),CC(13)
27	A″	-	1176	1037	1194	13.99	1.50	1045	1181	15.09	1.41	CH3opb(68)
28	A′	1171	-	1003	1184	3.49	23.35	1020	1176	0.06	10.10	bCH(64), CC(23)
29	A′	1115	-	968	1135	8.90	0.32	989	1124	12.75	2.04	CH3ipr(70)
30	A″	1105	-	865	1123	9.72	13.84	944	1101	8.85	14.74	CH3opr(68)
31	A″	842	847	848	857	10.71	10.14	852	835	8.97	9.11	ω CC(59)
32	A″	-	824	841	841	87.23	0.44	847	817	99.19	0.43	ωCH(58), ωCC(23)
33	A″	748	-	764	766	11.97	9.88	824	752	14.20	11.06	ωCH(56), bCC(17)
34	A″	715	-	720	734	18.53	25.09	740	720	25.14	19.49	tRtrig(60), ωCH(21)
35	A′	-	647	675	663	46.02	252.64	692	644	50.19	195.45	bCO(64), OH(22)
36	A″	539	-	641	552	25.30	94.58	671	545	32.65	82.86	ωOH(59), ωCO(27)
37	A′	501	-	528	513	22.76	58.85	472	498	29.24	59.01	tRasym(53),tRtrig(21)
38	A″	-	471	493	485	20.37	64.31	430	468	21.14	55.51	ωCH(55), Rsym(19)
39	A″	-	453	432	464	21.10	69.23	423	455	20.64	68.58	ωCO(59), tRasym(21)
40	A″	-	343	392	355	21.32	140.53	338	347	24.20	124.05	ωCH(57), ωCC(15)
41	A″	-	282	385	292	7.48	142.03	307	277	8.38	129.11	tRsym(55), ωCO(27)
42	A″	-	178	218	189	37.74	138.50	290	180	69.30	102.77	tCH3(60)

Table 10. Electric dipole moment, Polarizability and hyperpolarizability of *o*-cresol, *m*-cresol and *p*-cresol by DFT/B3LYP /6-311++G(d,p) level.

Parameters	***o*-cresol**	***m*-cresol**	***p*-cresol**
Polarizability(α)			
α_{xx}	-40.2964	-71.1963	-50.3694
α_{yy}	-49.304	-59.0299	-39.4555
α_{zz}	-52.3168	-68.3713	-52.3289
α_{xy}	2.7464	-6.4221	-1.059
α_{xz}	-0.0017	-4.0487	0.0013
α_{yz}	0.0009	-2.1194	-0.001
$\bar{\alpha}$	-47.305733	-66.199167	-47.3846
Anisotropic tensor			
A	234.703838	243.263668	288.677281
B	7.54271666	62.1271965	1.12148369
C	139.980069	308.013423	147.703092
Hyper polarizability (β)			
β_{xxx}	-15.3783	18.5339	-14.7137
β_{yyy}	-8.4011	-4.3882	-13.6026
β_{zzz}	0.003	-1.2737	0.0009
β_{xyy}	6.9832	15.7699	14.1862
β_{yxx}	3.2519	-1.557	-1.3381
β_{zxx}	0.004	7.9388	0.0035
β_{xzz}	-7.2427	-4.8856	1.6876
β_{yzz}	2.133	-8.532	-4.8144
β_{zyy}	-0.0004	-3.0052	0.0013
β_{x}	-15.6378	29.4182	1.1601
β_{y}	-3.0162	-14.4772	-19.7551
β_{z}	0.0066	3.6599	0.0057
β_{Total} x 10^{-30} cm^5esu^{-1}	2.1855	9.3765	3.3734

Table 11. Global and local reactivity descriptors and related molecular properties of HF and DFT/B3LYP/6-311++G(d,p) level for *o*-cresol, *m*-cresol and *p*-cresol.

Molecular Properties	***o*-cresol**		***m*-cresol**		***p*-cresol**	
	6-311++G(d,p)		**6-311++G(d,p)**		**6-311++G(d,p)**	
	HF	**B3LYP**	**HF**	**B3LYP**	**HF**	**B3LYP**
Ionisation potential (I)	-0.31958	-0.23284	-0.31958	-0.23339	-0.31295	-0.22858
Electron Affinity (A)	-0.03732	-0.01774	-0.03732	-0.01478	-0.03686	-0.01837
Global Hardness (η)	-0.14113	-0.10755	-0.14113	-0.109305	-0.138045	-0.105105
Electronegativity (χ)	-0.17845	-0.12529	-0.17845	-0.124085	-0.174905	-0.123475
Global softness (s)	-7.08566	-9.298000	-7.08566	-9.148712	-7.244015	-9.514295
Chemical potential (μ)	0.17845	0.12529	0.17845	0.124085	0.174905	0.123475
Global Electrophilicity (ω)	-0.112819	-0.0729780	-0.112819	-0.0704317	-0.110804	-0.072527

$$\chi = -\mu = -\mu = \left(\frac{\partial E}{\partial N}\right)_{v(r)}$$

where E and *v*(r) are electronic energy and external potential of an N-electron system respectively. Softness is a property of compound that measures the extent of chemical reactivity. It is the reciprocal of hardness.

$$S = \frac{1}{\eta}$$

Using Koopman's theorem for closed-shell compounds, η, μ and χ can be defined as,

$$\mu = \frac{(I - A)}{2}$$

$$\mu = \frac{-(I + A)}{2}$$

$$\chi = \frac{(I + A)}{2}$$

where A and I are the ionization potential and electron affinity of the compounds respectively. Electron affinity refers to the capability of ligand to accept precisely one electron from a donor. However in many kinds of bonding viz. covalent hydrogen bonding, partial charge transfer takes places.

Recently Parr et al. [60] have defined a new descriptor to quantity the global electrophilic power of the compound as electrophilicity index (ω), which defines a quantitative classification of global electrophilic nature of a compound. Parr et al. have also proposed electrophilicity index (ω) as a measure of energy lowering due to maximal electron flow between donor and acceptor. They defined electrophilicity index (ω) as follows.

$$\omega = \frac{\mu^2}{2\eta}$$

The usefulness of this new reactivity quantity has been recently demonstrated in understanding the toxicity of various pollutants in terms of their reactivity and site selectivity [65–67]. The calculated value of electrophilicity index describes the biological activity of o-cresol, m-cresol and p-cresol. All the calculated values of hardness, potential, softness and electrophilicity index are shown in Table 11.

Conclusion

A complete structural, thermodynamic, vibrational and electronic investigations along with FTIR, FT-Raman, and natural bond orbital analysis of *o*-cresol, *m*-cresol and *p*-cresol have been carried out with *ab initio* HF and DFT/B3LYP method. The FTIR and FT-Raman spectra have been recorded and analysed. NBO atomic charges are obtained with DFT/B3LYP with 6-31++G(d,p) basis set. The temperature dependence of thermodynamic parameters in the range 100^0-1000^0 K were determined and found that all thermodynamic properties increase with rise in temperature. A close agreement has been noticed between the experimental and theoretical values of wavelength.

References

[1] S. M. Kumbar, G.V. Shanbhag, F. Lefebvre, S.B. Halligudi, J. Mol. Cat. A: Chem.
256 (2006) 324–334.
[2] M. Misono, T. Okuhara, Chemtech 23 (11) (1993) 23-34.
[3] J.M. Thomas, Sci. Am. 112 (1992) 2664-2673.
[4] J. Pospisil, Poly. Deg. Stab. 20 (1988) 181-196.
[5] Z.X. Su, T.J. Wang, React. Funct. Polym. 28 (1995) 97-107.
[6] A.M. Bruce, H. Smith, A.A. Watson, Med. Sci. Law, 16(3) (1976) 171-177.
[7] M.A. Green, Med. Sci. Law, 15(1) (1975) 65-73.
[8] L. Morris, D. Bergner, A. Mencher, J. Chem. Phys. 845 (1943) 136- 148.
[9] Y. Morinaga, C. Fuke, T. Arao, T. Miyazaki , J. Forensic. Sci. 6 (2004) 32–40.
[10] A.P. Hart, A. Dasgupta, J. Forensic. Sci. 42(4) (1997) 693-699.
[11] L. Dou, C. Cerini, P. Brunet, C. Guilianelli, V. Rie moal, G. Grau, R. De smet, R. Vanholder, J. Sampol, Y. Berland, Kidney International, 62 (2002)1999–2009.
[12] B. Bammens1, P. Evenepoel1, H. Keuleers, K. Verbeke, Y. Vanrenterghem1, Kidney International 69 (2006) 1081–1087.
[13] L. Dou, E. Bertrand, C. Cerini, V. Faure, J. Sampol, R. Vanholder, Y. Berland, P. Brunet, Kidney International, 65 (2004) 442–451.
[14] R. Vanholder, R. De smet, M.A. Waterloos, N.V. Landschoot, P. Vogeleere, E. Hoste, S. Ringir, Kidney International, 47 (1995) 510—517.
[15] V.F. Bergerova, J.T. Pierce, P.O. Droz, journal of catalysis, 17 (1990)617–635.
[16] Recommendation from the scientific committee on occupational exposure limits for cresol (all isomers) 96 march 2002.
[17] R. I. Olariu, B. Klotz, I. Barnes, K.H. Becker, R. Mocanu, Nephrol Dial Transplant 69(2001)516–522.
[18] H.J. Oneill, C. Mccaughey, P.V. Coyle, D.E. Wyatt, F. Mitchell, J.Mol.Struct october 70(1997) 334-340.
[19] R. Vanholder , R. De smet, R. Glorieux, A. Argilés, U. Baurmeister, P. Brunet, Kidney International 63(2003)1934-1943.
[20] R. Vanholder, R. De smet, G. Lesafferg. nephrol dial transplant 14(1999) 2813-2815.
[21] V. Umamaheswari, M. Palanichamy, V. Murugesa, Journal of catalysis 210(2002) 367–374
[22] M.J. Frisch, G.W. Trucks, H.B. Schlegel, G.E. Scuseria, M.A. Robb, J.R. Cheeseman, J.A. Montgomery Jr., T. Vreven, K.N. Kudin, J.C. Burant, J.M. Millam, S.S. Iyengar,J. Tomasi, V. Barone, B. Mennucci, M. Cossi, G. Scalmani, N. Rega, G.A. Petersson, H. Nakatsuji, M. Hada, M. Ehara, K. Toyota, R. Fukuda, J. Hasegawa, M. Ishida, T. Nakajima, Y. Honda, O. Kitao, H. Nakai, M. Klene, X. Li, J.E. Knox, H.P. Hratchian, J.B. Cross, C. Adamo, J. Jaramillo, R. Gomperts, R.E. Stratmann, O. Yazyev, A.J. Austin, R. Cammi, C. Pomelli, J.W. Ochterski, P.Y. Ayala, K. Morokuma, A. Voth, P. Salvador, J.J. Dannenberg, V.G. Zakrzewski, S. Dapprich, A.D. Daniels, M.C. Strain, O. Farkas, D.K. Malick, A.D. Rabuck, K. Raghavachari, J.B. Foresman, J.V. Ortiz, Q. Cui, A.G. Baboul, S. Clifford, J. Cioslowski, B.B. Stefanov, G. Liu, A. Liashenko, P. Piskorz, I. Komaromi, R.L. Martin, D.J. Fox, T. Keith, M.A. Al-Laham, C.Y. Peng, A. Nanayakkara, M. Challacombe, P.M.W. Gill, B. Johnson, W. Chen, M.W. Wong, C. Gonzalez, J.A. Pople, Gaussian Inc., Wallingford, CT, 2004.
[23] M.J. Frisch, A.B. Nielsen, A.J. Holder, Gauss View Users Manual, Gaussian Inc., Pittsburgh, PA, 2000.
[24] E.B. Wilson Jr., J. Chem. Phys. 7 (1939) 1047–1052.
[25] E.B. Wilson Jr., J. Chem. Phys. 9 (1941) 76–84.
[26] E.B. Wilson Jr., J.C. Decius, P.C. Cross, Molecular Vibrations, McGraw Hill, New York, 1955.

[27] H. Fuhrer, V.B. Kartha, K.L. Kidd, P.J. Kruger, H.H. Mantsch, Computer Program for Infrared and Spectrometry, Normal Coordinate Analysis, vol. 5, National Research Council, Ottawa, Canada, 1976.
[28] V. Krishnakumar, G. Keresztury, T. Sundius, R. Ramasamy, J. Mol. Struct. 702 (2004) 9–21.
[29] J.S. Murray, K. Sen, Molecular Electrostatic Potentials, Concepts and Applications, Elsevier, Amsterdam, 1996.
[30] S. Chidangil, M.K. Shukla, P.C. Mishra, J. Mol. Modell. 4 (1998) 250–258.
[31] A.E. Frisch, H.P. Hratchian, R.D. Dennington II, et al., GaussView, Version 5.0.8, Gaussian, Inc., 235 Wallingford CT, 2009.
[32] I. Fleming, Frontier Orbitals and Organic Chemical Reactions, John Wiley and Sons, New York, 1976. pp. 5–27.
[33] E. Runge, E.K.U. Gross, Phys. Rev. Lett. 52 (1984) 997–1000.
[34] F. Furche, R.J. Ahlrichs, J. Chem. Phys. 117 (2002) 7433–7447.
[35] R. Bauernschmitt, R. Ahlrichs, Chem. Phys. Lett. 256 (1996) 454–464.
[36] C. Jamorski, M.E. Casida, D.R. Salahub, J. Chem. Phys. 104 (1996) 5134–5147.
[37] Z. Ran, D. Baotong, S. Gang, S. Yuxi, Spectrochim. Acta 75A (2010) 1115–1124.
[38] G. Wang, F. Lian, Z. Xie, G. Zu, L. Wang, X. Ring, F. Wang, Synth. Met. 131 (2002) 1–5.
[39] M. Amalanathan, V.K. Rastogi, I.H. Joe, M.A. Palafox, R. Tomar, Spectrochim. Acta A78 (2011) 1437 – 1444.
[40] L. Padmaja, C. Ravikumar, D. Sajan, I.H. Joe, V.S. Jayakumar, G.R. Pettit, J. Raman Spect. 40 (2009) 419 – 428.
[41] M. Karabacak, M. Cinar, M.Kurt, J.Mol. Struct. 885(2008) 28-35.
[42] A.P. Scott, L. Radom . J. Phys. Chem 100(1996) 16502-16513.
[43] H.F. Hameka, J.O. Jensen, J. Mol. Struct(Theochem) 362 (1996) 325-330.
[44] C. P. Vlahacor, H.P. Hameka, J.O. Jensen, Chem.Phys. Lett. 259(1996) 283- 286.
[45] D. Zeroka, J.O. Jensen, J. Mol.Struct(Theo.Chem) 425(1998) 181-192.
[46] K.K. Ong, J.O. Jensen, H.F. Hameka, J.Mol.Struct (TheoChem). 459(1999) 131-144.
[47] J.O. Jensen, A. Banerjee, C.N. Merrow, D. Zeroka. J.M. Lochner, J. Mol. Struct(Theochem) 531(2000) 323-331.
[48] M.W. Eillzy, J.O. Jensen, H.F. Hameka, J.G. Kay, D.Zeroka, Spectrochim. Acta 57A (2001) 2417-2432.
[49] H.F. Hameka, J.O. Jensen, J. Mol. Struct.(Theochem) 331(1995) 203-214.
[50] J.O. Jensen, D.Zeroka, J.Mol.Struct.(Theochem) 487(1999) 267-274.
[51] A. Cheoperana, P. Painter, Vib.Spectrosc. 51(2009) 110-124.
[52] R.M. Silverstein, G.C. Bassler, T.C. Morrill, Spectrometric Identification of Organic Compounds, 5th ed., John Wiley & Sons, New York. p.245.
[53] B. Smith, Infrared Spectral Interpretation, A Systematic approach, CRC Press, Washington, DC, 1989.
[54] G. Varsanyi, Assignments for Vibrational Spectra of Seven Hundred Benzene Derivatives, Vols 1 and 2, Academic Kiado, Budapest, 1973.
[55] M. Jag, Organic Spectroscopy-Principles and Applications, 2nd ed., Narosa Publishing house, New Delhi. 2001.
[56] J.B. Lambert, H.F. Shurvell, L. Verbit, R.G. Cooks, G.H. Stout, Organic Structural Analysis, Macmillan Publ.Co.Inc., New York, 1976.
[57] J. Mohan, Organic Spectroscopy – Principles and Applications, Narosa Publishing, New Delhi, 2001.
[58] G. Socrates, Infrared Characteristic Frequencies, Wiley Inter Science Publication, New York, 1990.
[59] M. Silverstein, G. Clayton Basseler, C. Morill, Spectrometric Identification of Organic Compounds, Wiley, New York, 1981.
[60] R.G. Parr, L.V. Szentpaly, S.J. Liu, Am. Chem. Soc. 121 (1999) 1922 – 1924.
[61] P.K. Chaltraj, B. Maiti, U.J. Sarbar, J. Phys. Chem. A 107 (2003) 4973 - 4977.
[62] R.G. Parr, R.A. Donnelly, M. Levy, W.E. Palke, Am. Chem. Soc. 68 (1978) 3801–3807.
[63] R.G. Parr, R.G. Pearson, J. Am. Chem. Soc. 105 (1983) 7512–7516.
[64] R.G. Parr, P.K. Chattraj, J. Am. Chem. Soc. 113 (1991) 1854–1855.
[65] R. Parthasarathi, J. Padmanabhan, V. Subramanian, B. Maiti, P.K. Chattraj, J. Phys.Chem. A 107 (2003) 10346–10352.
[66] R. Parthasarathi, J. Padmanabhan, V. Subramanian, B. Maiti, P.K. Chaltraj, Curr. Sci. 86 (2004) 535–542.
[67] R. Parthasarathi, J. Padmanabhan, V. Subramanian, U. Sarkar, B. Maiti, P.K. Chattraj, Internet Electron. J. Mol. Des. 2 (2003) 798–813.